IEEE Access
Multidisciplinary | Rapid Review | Open Access Journal

Received July 25, 2021, accepted August 5, 2021, date of publication August 12, 2021, date of current version August 18, 2021.

Digital Object Identifier 10.1109/ACCESS.2021.3104301

A Predictive Torque Control Method for Dual Three-Phase Permanent Magnet Synchronous Motor Without Weighting Factor

ZHIFENG ZHANG, (Member, IEEE), QUANZENG SUN, QISHEN DI, AND YUE WU
School of Electrical Engineering, Shenyang University of Technology, Shenyang 110870, China

Corresponding author: Quanzeng Sun (1074287890@qq.com)

This work was supported by the National Natural Science Foundation of China Study on Fault Diagnosis and Fault-Tolerant Control of Multi-Phase Motor Drive Control System for Electric Vehicle under Grant 61603263.

ABSTRACT In order to solve the problem of the difficult design of weighting factor for model predictive torque control (MPTC) of dual three-phase permanent magnet synchronous motor (DT-PMSM), this paper proposes a MPTC strategy without weighting factor. Firstly, the virtual voltage vector (V^3) is introduced to reduce the harmonic currents. Secondly, an approximate alternative principle for predicted current is proposed, which simplifies the dual-vector prediction model and decreases the complexity of the prediction model. The control set at $(k+1)$th is selected by judging the change in torque and the position of the stator flux, which reduces the number of candidate voltage vectors. Thirdly, the cost function is selected according to the system state at two adjacent moments. The cost function separates the electromagnetic torque and the stator flux, and eliminates the weighting factor. Decreasing the complexity of the prediction model, reducing the number of candidate voltage vectors, the combination of the two methods in this paper can significantly reduce the computational burden of the CPU. Finally, experiments verify the effectiveness of the proposed method. The results show that the proposed method greatly reduces the calculation burden of the system under the performance of electromagnetic torque does not change much.

INDEX TERMS Dual three-phase permanent magnet synchronous motor, model predictive torque control, weighting factor, torque ripple, harmonic current.

I. INTRODUCTION

Recently, more and more researches on DT-PMSMs have been conducted. Compared with three-phase motors, DT-PMSMs have the characteristics of higher torque density, better fault tolerance, and lower torque ripple [1]–[3].

Sliding mode control [4]–[7], fuzzy control [8], [9], and model predictive control (MPC) [10] are used in different fields due to their respective advantages. Among them, MPC has developed rapidly in recent years. MPC technology has been applied to motors, and the performance of the motors is very outstanding [11]–[15]. The advantages of MPC are simpler control structure [16], fast response speed [17], and easy to modify the restriction conditions [18]. MPC has become the most important control method after vector control and direct torque control. The conventional MPC includes three main parts: 1) Collect the physical quantities at the present moment; 2) Use the prediction model to predict the control results of each control set; 3) Evaluate the prediction results of the control set through the cost function, and screen out the optimal control set to be used in the next control period.

In the three processes described above, the control sets and the cost function can directly affect the control effect of the system. The greater the number of control sets and the more accurate the design cost function, the better the control results obtained. Too many control sets or complex design cost functions lead to a heavier computational burden on the system. Therefore, the rationality of the design of the two is particularly important. Compared with the conventional three-phase motor MPC system, all control sets are predicted in each control period, while the multi-phase motor control sets are more. Predicting all control sets will generate a huge amount of calculation [19]–[21]. As a result, the calculation load of the microprocessor in a control period is significantly

The associate editor coordinating the review of this manuscript and approving it for publication was Mauro Gaggero.

increased. At the same time, using the principle of space vector decoupling, the control set can be decomposed into three mutually orthogonal planes. If the basic voltage vector is directly used as the control set, which will cause the motor to generate large harmonic currents [20]–[23], the harmonic current will reduce the control performance of the system. In summary, harmonic current and the computational burden have become key issues in MPC method of multi-phase motors.

[24]–[30] propose improvement methods to solve the problem of large harmonic currents. [27], [28] introduce the V^3 method to suppress harmonic currents, which have verified the effectiveness of the V^3 method, but calculation burden increases, and the switching frequency is increased to a certain extent. The prediction of the voltage vector will generate a lot of calculations. In [29]–[31], only the basic voltage vector with the largest amplitude is introduced as the control set for prediction, which not only does not use the abundant voltage vector of the multi-phase motor but also reduces the control performance of the system. [32] introduces a voltage vector screening method by direct torque control, using a voltage vector switching table to complete the optimal voltage vector screening. However, this method does not simplify the prediction model, which will cause a sudden increase in the complexity of the calculation. [33] introduces a MPC method without weighting factors. This method only evaluates the magnitude of the V^3, but it is difficult to realize for MPTC. In [34], the V^3 method and duty period optimization methods are used to simplify the cost function, and only the stator flux and current limit are evaluated in the cost function, thereby avoiding the adjustment of the weighting factor. [35] proposes a dual-vector MPC method, and introduces geometric principles to eliminate the weighting factor of the cost function. The proposed method reduces the computational burden. [36] introduces a novel predictive control method of duty period without weighting factor, which simplifies the cost function to only the stator flux component. Compared with [34], the current limit is eliminated, and the computational burden is also reduced.

This paper focuses on harmonic currents, torque ripple and calculation burden in the DT-PMSM predictive control method. A MPTC method without a weighting factor is proposed. Firstly, the V^3 method is introduced to suppress the harmonic currents. Secondly, the prediction model based on the dual-vector is simplified, and the complexity of the prediction model is decreased. Reduce the number of candidate voltage vectors by judging the change in torque and the position of the stator flux linkage, which reduces the computational burden. Thirdly, the cost function is adjusted according to the system state, which eliminates the weighting factor.

The remaining structure of the paper is as follows: in Section II, the mathematical model of the DT-PMSM based on the VSD transform and the conventional model predictive torque control is presented, and in Section III, the specific details of the proposed method and the structural block diagram of the method are presented. In Section III, experimental results are given. Finally, conclusions are made in section V.

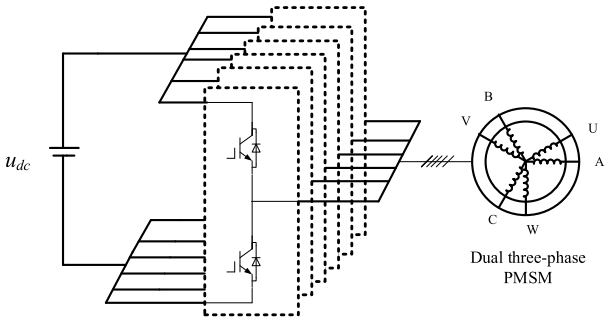

FIGURE 1. Scheme of DT-PMSM.

II. CONVENTIONAL MPTC SCHEME

A. PREDICTION MODEL

The spatial structure of the DT-PMSM stator coil and the connection between the six-arm two-level inverter are shown in Fig.1.The two sets of stator windings have two independent nodes. u_{dc} is the DC voltage. DT-PMSM is modeled using Vector Space Decomposition (VSD), and the VSD transformation matrix is expressed as (1):

$$T_{\alpha\beta} = \frac{1}{3}\begin{bmatrix} 1 & -\frac{1}{2} & -\frac{1}{2} & \frac{\sqrt{3}}{2} & -\frac{\sqrt{3}}{2} & 0 \\ 0 & \frac{\sqrt{3}}{2} & -\frac{\sqrt{3}}{2} & \frac{1}{2} & \frac{1}{2} & -1 \\ 1 & -\frac{1}{2} & -\frac{1}{2} & -\frac{\sqrt{3}}{2} & \frac{\sqrt{3}}{2} & 0 \\ 0 & -\frac{\sqrt{3}}{2} & \frac{\sqrt{3}}{2} & \frac{1}{2} & \frac{1}{2} & -1 \\ 1 & 1 & 1 & 0 & 0 & 0 \\ 0 & 0 & 0 & 1 & 1 & 1 \end{bmatrix} \tag{1}$$

In order to obtain the synchronous frame structure, Park transformation is applied to the $d-q$ plane:

$$T_{dq} = \begin{bmatrix} \cos\theta & \sin\theta \\ -\sin\theta & \cos\theta \end{bmatrix} \tag{2}$$

$$\begin{bmatrix} v_d & v_q \end{bmatrix}^T = T_{dq}\begin{bmatrix} v_\alpha & v_\beta \end{bmatrix}^T \tag{3}$$

where θ represents the angle of the d axis of the rotor relative to the α axis. By using this method, the model of the DT-PMSM can be obtained in the synchronous reference frame and x-y plane is as follows:

$$\begin{bmatrix} v_d \\ v_q \end{bmatrix} = \begin{bmatrix} R & -\omega_r L_q \\ \omega L_d & R \end{bmatrix}\begin{bmatrix} i_d \\ i_q \end{bmatrix} + \begin{bmatrix} L_d \\ L_q \end{bmatrix} {}^*p^* \begin{bmatrix} i_d \\ i_q \end{bmatrix} + \begin{bmatrix} 0 \\ \omega\psi_f \end{bmatrix} \tag{4}$$

$$\begin{bmatrix} v_x \\ v_y \end{bmatrix} = \begin{bmatrix} R & 0 \\ 0 & R \end{bmatrix}\begin{bmatrix} i_x \\ i_y \end{bmatrix} + L_l {}^*p^* \begin{bmatrix} i_x \\ i_y \end{bmatrix} \tag{5}$$

$$\begin{bmatrix}\psi_d\\ \psi_q\\ \psi_x\\ \psi_y\end{bmatrix}=\begin{bmatrix}L_d & 0 & 0 & 0\\ 0 & L_q & 0 & 0\\ 0 & 0 & L_{ls} & 0\\ 0 & 0 & 0 & L_{ls}\end{bmatrix}\begin{bmatrix}i_d\\ i_q\\ i_x\\ i_y\end{bmatrix}+\psi_f\begin{bmatrix}1\\ 0\\ 0\\ 0\end{bmatrix} \tag{6}$$

$$T_e=3n_p\left[\psi_d i_q-\psi_q i_d\right] \tag{7}$$

where V_d, V_q represent the stator voltage components in the d-and q-axis; i_d, i_q represent the stator current components in the d-and q-axis; R is the stator resistance; L_d, L_q represent the stator inductances in the d-and q-axis. ψ_x, ψ_y represent the flux in the x-y plane; ψ_f represents the permanent magnet flux; V_x, V_y are the stator voltage components in the x-y plane; i_x and i_y are the stator current components in the x-y plane; ω is the rotor angular velocity; P is the time derivative operator; L_{ls} is the leakage self-inductance, T_e is the electromagnetic torque, and n_p is the number of pole pairs.

B. LINEAR DISCRETIZATION AND COST FUNCTION

According to the conventional Finite-Control-Set MPC control principle, the predicted current at the $(k+1)$th is shown as:

$$\begin{cases} i_s(k+1)=i_s(k)+\dfrac{T_s}{L_s}\left(u_s-R_s i_s(k)\right)+e_{dq}\\ \psi_s(k+1)=T_s u_s(k)+\left(1-\dfrac{R_s}{L_d}T_s\right)\psi_s(k)+\psi_{dq}\\ i_s=\begin{bmatrix}i_d & i_q\end{bmatrix}^T\\ L_s=\begin{bmatrix}L_d & L_q\end{bmatrix}^T\\ e_{dq}=\left[\omega L_q i_q-\omega\left(L_d i_d+\psi_f\right)\right]^T\\ \psi_s=\begin{bmatrix}\psi_d & \psi_q\end{bmatrix}^T\\ \psi_{dq}=\left[\omega\psi_q T_s+\dfrac{R_s}{L_d}T_s\psi_f-\omega\psi_d\right]^T \end{cases} \tag{8}$$

Based on the current prediction model and the stator flux prediction model, the torque prediction model can be obtained as:

$$T_e(k+1)=3n_p\left(\psi_d(k+1)i_q(k+1)-\psi_q(k+1)i_d(k+1)\right) \tag{9}$$

The cost function of conventional MPTC is usually composed of electromagnetic torque and stator flux at kth and $(k+1)$th directly, and the purpose is to select the optimal switching state. The calculation of electromagnetic torque and stator flux at $(k+1)$th is introduced in [36]. The cost function can be expressed as:

$$J=\left|T_e^*-T_e(k+1)\right|+\lambda\left|\psi_s^*-\psi_s(k+1)\right| \tag{10}$$

Among them, T_e^* and ψ_s^* are the reference electromagnetic torque and stator flux, and λ is the weighting factor used to balance the influence of electromagnetic torque and stator flux. The design of the weighting factor is a relatively tedious task.

C. PREDICTIVE VOLTAGE VECTORS

The DT-PMSM is powered by a six-phase voltage source inverter, which has a total of $2^6 = 64$ switching states [$S_A S_B S_C S_U S_V S_W$], where $S_i = 1$ (i = A,B,C,U,V,W) when the upper arm is ON; $S_i = 0$ (i = A,B,C,U,V,W) when the lower arm is ON. Each switch state corresponds to a basic voltage vector in both planes. The 64 switching states of the inverter are arranged according to the binary numbers. For example, V_{13} means 001101, which means that the lower bridge arm of phase A, B and V is ON, and the upper bridge arm of phase C, U and W is ON. Among the 64 states of the inverter, there are 60 active basic voltage vectors and four zero voltage vectors are V_0, V_7, V_{56} and V_{63}. The active voltage vectors can be categorized into four groups: $G_1(0.644u_{dc})$, $G_2(0.47u_{dc})$, $G_3(0.331u_{dc})$, and $G_4(0.172u_{dc})$.

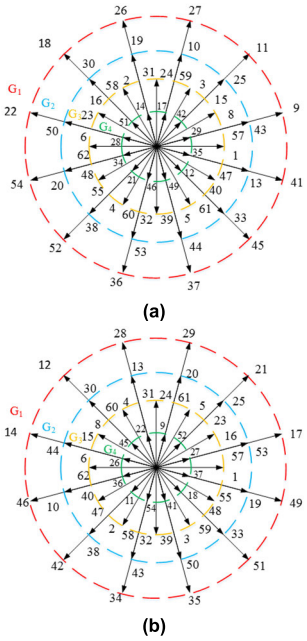

FIGURE 2. Basic voltage vectors in the (a) x-y plane and (b) z_1–z_2 plane.

The 64 basic voltage vectors of the six-bridge arm inverter can be distributed in three mutually orthogonal planes, x-y, z_1-z_2, and o_1-o_2, where the o_1-o_2 plane is zero. The basic voltage vector distribution is shown in Fig.2. Evaluating all 64 voltage vectors is redundant. The usual method is to evaluate the 12 basic voltage vectors with the largest amplitude, and then use them in the cost function at the next moment.

III. PRINCIPLE OF THE PROPOSED MPTC METHOD

A. SYNTHESIZATION OF PREDICTION VECTORS

The advantage of the DT-PMSM is that the voltage vector is abundant, which provides a new way for harmonic currents suppression. Use the V^3 method to solve the related problems of harmonic currents. According to (5), it can be seen that zero voltage determines zero current. Therefore, the amplitude of the V^3 is equal to zero in the z_1-z_2 plane. It can be seen from Fig.2 (a) that the amplitudes of V_{27} and V_{10} are

different, but the phases are the same, which means that V_{27} and V_{10} have the same effect on electromagnetic torque and stator flux.

V_{27} and V_{10} are opposite directions in the z_1-z_2 plane, so the two have opposite effects in terms of harmonic effects. Similarly, the voltage vectors of the G1 and G2 groups also have these characteristics. Therefore, the voltage vectors of G1 and G2 are used to synthesize V^3s. The calculation of the V^3 synthesized by V_{27} and V_{10} is as follows:

$$\begin{cases} \eta_1 |V_{27}| - \eta_2 |V_{10}| = 0 \\ \eta_1 + \eta_2 = 1 \end{cases} \tag{11}$$

η_1 and η_2 are obtained by calculation;

$$\eta_1 = 0.269, \quad \eta_2 = 0.731 \tag{12}$$

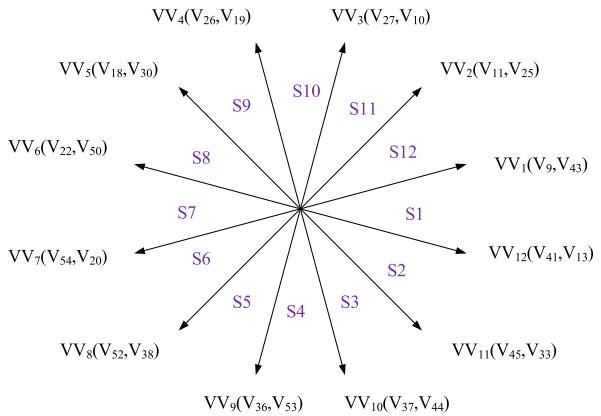

FIGURE 3. Spatial distribution of V^3s.

Fig.3 shows the spatial distribution of the V^3s. The amplitude of the V^3 is $0.597u_{dc}$. Similarly, the V^3 is synthesized by G_2 and G_4, which can also have the effect of harmonic suppression, but the amplitude of V^3 is $0.345u_{dc}$. And the voltage utilization rate is reduced by about 25%, so G1 is most suitable for synthesizing V^3 with G2.

B. SIMPLIFICATION OF PREDICTION MODEL

The prediction model based on the dual-vector is shown in (13).

$$\begin{cases} i_d(k+1) = \left(1 - \dfrac{R_s T_2}{L_d}\right)\left(\left(1 - \dfrac{R_s T_1}{L_d}\right) i_d(k) \right. \\ \quad \left. + T_1 \omega i_q(k) + \dfrac{T_1}{L_d} u_{d1}(k)\right) \\ \quad + T_2 \omega \left(\left(1 - \dfrac{R_s T_1}{L_q}\right) i_q(k) - T_1 \omega i_d(k) \right. \\ \quad \left. - \dfrac{1}{L_q} \psi_f \omega T_1 + \dfrac{T_1}{L_q} u_{q1}(k)\right) + \dfrac{T_2}{L_d} u_{d2}(k) \\ i_q(k+1) = \left(1 - \dfrac{R_s T_2}{L_q}\right)\left(\left(1 - \dfrac{R_s T_1}{L_q}\right) i_q(k) - T_1 \omega i_d(k) \right. \\ \quad \left. - \dfrac{1}{L_q} \psi_f \omega T_1 + \dfrac{T_1}{L_q} u_{q1}(k)\right) - T_2 \omega \left(\left(1 - \dfrac{R_s T_1}{L_d}\right) i_d(k) \right. \\ \quad \left. + T_1 \omega i_q(k) + \dfrac{T_1}{L_d} u_{d1}(k)\right) - \dfrac{1}{L_q} \psi_f \omega T_2 + \dfrac{T_2}{L_q} u_{q2}(k) \end{cases} \tag{13}$$

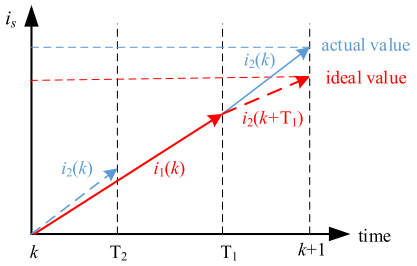

FIGURE 4. Approximate schematic.

where $T = T_1 + T_2$, T_1 and T_2 represent the action time of the two vectors. From (13), it can be seen that the conventional prediction model using the V^3 method is very computationally intensive. An approximate alternative principle will be used to calculate the predicted current, and the schematic diagram is given in Fig.4.

In Fig.4, $i_1(k)$ is the effect of u_1 acting alone on i_s within T_1, $i_2(k)$ is the effect of u_2 acting alone on i_s within T_2. $i_2(k+T_1)$ is the effect of u_2 acting on $i_s(k+T_1)$ within T_2 after the effect of u_1 acting on i_s. Regardless of the interaction of the two voltage vectors in one control period, only the individual effect of the two voltage vectors on the motor is considered. Use $i_2(k)$ instead of $i_2(k+T_1)$ to synthesize approximate current values. According to this principle, all terms of T_1 and T_2 multiplication in the original prediction current model can be omitted. Since T_1 and T_2 multiplication values in one sampling period are very little, the current error will not be very large. The ideal value is the current value before simplification and the actual value is the current value after simplification. The current value at $(k+1)$th can be expressed in (14).

$$\begin{cases} i_s(k+1) = i_s(k) + s_1 T_1 + s_2 T_2 \\ s_1 = \left.\dfrac{di_s(k)}{dt}\right|_{u_s=u_1} = \dfrac{T_s}{L_s}(u_1 - R_s i_s(k)) + e_{dq} \\ s_2 = \left.\dfrac{di_s(k)}{dt}\right|_{u_s=u_2} = \dfrac{T_s}{L_s}(u_2 - R_s i_s(k)) + e_{dq} \end{cases} \tag{14}$$

The current prediction model can be obtained after simplification:

$$\begin{cases} i_d(k+1) = i_d(k) \\ \quad + \dfrac{1}{L}(u_{d1} T_1 + u_{d2} T_2 - R_s i_d T_s + \omega L i_q T_s) \\ i_q(k+1) = i_q(k) \\ \quad + \dfrac{1}{L}(u_{q1} T_1 + u_{q2} T_2 - R_s i_q T_s + \omega L i_d T_s - \omega \psi_f) \end{cases} \tag{15}$$

Compared with (13), (15) is much simpler, which used the approximation principle. Similarly, a simplified model of the stator flux can be obtained:

$$\begin{cases} \psi_d(k+1) = T_1 u_{d1}(k) + T_2 u_{d2}(k) + \left(1 - \dfrac{R_s}{L} T_s\right) \psi_d(k) \\ \quad + \omega \psi_q(k) T_s + \dfrac{R_s}{L} T_s + \dfrac{R_s}{L} T_s \psi_f \\ \psi_q(k+1) = T_1 u_{q1}(k) + T_2 u_{q2}(k) + \left(1 - \dfrac{R_s}{L} T_s\right) \psi_q(k) \\ \quad - \omega \psi_d(k) T_s \end{cases} \tag{16}$$

C. SIMPLIFICATION OF CONTROL SETS AND ELIMINATION WEIGHTING FACTOR

From (17), the influence of voltage vector on electromagnetic torque and stator flux can be obtained.

$$\begin{cases} \dfrac{dT_e}{dt} = -\dfrac{R_s}{L_s}T_e - \dfrac{3p}{L_s}\omega\psi_s\psi_f\cos\delta + \dfrac{3p}{L_s}\psi_f V_{sy}\cos\delta \\ \dfrac{d\psi_s}{dt} = u_s T_s \cos\theta_{u_s\psi_s} \end{cases} \tag{17}$$

where δ is the electromagnetic torque angle, $\theta_{u_s\psi_s}$ is the angle between the voltage vector and the stator flux.

It can be seen from (17) that the voltage vector affects the change of stator flux and torque. When the angle between the voltage vector and the stator flux is less than 90°, the amplitude of the stator flux increases; if the angle is greater than 90°, the amplitude of the stator flux decreases. When the voltage vector and the stator flux rotate in the same direction and the angle between the two is less than 180°, the amplitude of electromagnetic torque increases; when the voltage vector and the stator flux rotate in the opposite direction and the angle between the two is less than 180°, the amplitude of electromagnetic torque decreases.

TABLE 1. System states judgment.

System States	$\lvert T_e^*\text{-}T_e\rvert$ at (k-1)th	$\lvert T_e^*\text{-}T_e\rvert$ at k th
From dynamic to Steady state	More than B_T	Less than B_T
Dynamic	More than B_T	More than B_T
Steady state	Less than B_T	Less than B_T
From steady state to Dynamic	Less than B_T	More than B_T

The $T_e(k)$ at kth and the $T_e(k-1)$ at $(k-1)$th can be obtained through the control system, and the operating state of the system is judged according to the difference between the torque value and the reference torque value at the two moments. The basis for judging the system states is shown in Table 1, where B_T is the bandwidth of the torque hysteresis controller in direct torque control. It is specified that the torque is dynamic state when it needs to be changed, and steady state when it does not need to be changed. When $|T_e^*-T_e|$ is greater than B_T, the torque needs to be changed, and the system state is dynamic, and when $|T_e^*-T_e|$ is less than B_T, the torque does not need to be changed, and the system state is steady.

According to the torque error of the system at two moments, it can be divided into four states: from dynamic to steady state, dynamic state, steady state and from steady state to dynamic. These four states will be analyzed in detail below:

1) THE SYSTEM CHANGES FROM DYNAMIC TO STEADY STATE

If the system changes from dynamic to steady state, the voltage vector selected at $(k-1)$th will cause the torque to change rapidly at the next moment. At this time, the sector where the stator flux is located can be roughly judged based on the torque change after the voltage vector is applied. Assuming that the voltage vector selected at $(k-1)$th is V_1, the positions of the stator flux at $(k-1)$th are roughly S_3, S_4, S_9, and S_{10}. Assuming that the stator flux does not change in a control period, the sectors where the voltage vector selected at $(k+1)$th are S_3, S_4, S_9, and S_{10} according to the system state at kth. The candidate voltage vector is VV_3, VV_4, VV_5, VV_9, VV_{10}, VV_{11}. The method of selecting the control set is shown in Fig.5(a).

2) THE SYSTEM IS DYNAMIC STATE

If the system is dynamic state, the voltage vector selected at $(k-1)$th and kth will cause the torque to change rapidly at the next moment. The sector where the stator flux is located can be roughly judged. Assuming that the voltage vector selected at $(k-1)$th is V_1, the sectors where the stator flux is located at $(k-1)$th are S_3, S_4, S_9, and S_{10}. And assuming that the stator flux does not change in one control period, the sectors where the voltage vector selected at $(k+1)$th are S_1, S_6, S_7, and S_{12} according to the system state at kth. The candidate voltage vector is VV_2, VV_1, VV_{12}, VV_6, VV_7, VV_8. The method of selecting the control set is shown in Fig.5(b).

3) THE SYSTEM IS STEADY STATE

If the system has been in steady state. The voltage vector will not make the torque change rapidly. Assuming that the voltage vector selected at $(k-1)$th is V_1, the sectors where the stator flux is located at $(k-1)$th are S_1, S_6, S_7, and S_{12}. And assuming that the stator flux does not change in one control period, the sectors where the voltage vector selected at $(k+1)$th are S_1, S_6, S_7, and S_{12} according to the system state at kth. The candidate voltage vector is VV_2, VV_1, VV_{12}, VV_6, VV_7, VV_8. The method of selecting the control set is shown in Fig. 5(c).

4) THE SYSTEM CHANGES FROM STEADY STATE TO DYNAMIC

If the system changes from steady state to dynamic, the voltage vector selected at $(k-1)$th will not cause the torque to change rapidly. Assuming that the voltage vector selected at $(k-1)$th is V_1, the sectors where the stator flux is located at $(k-1)$th are roughly S_1, S_6, S_7, and S_{12}. Assuming that the stator flux does not change in a control period, the sectors where the voltage vector selected at $(k+1)$th are S_3, S_4, S_9, and S_{10} according to the system state at kth. The candidate voltage vector is VV_3, VV_4, VV_5, VV_9, VV_{10}, VV_{11}. The method of selecting the control set is shown in Fig.5(d).

When the system changes from dynamic to steady state, the voltage vector selected does not need to make a rapid change in torque, and the cost function does not contain the component of the torque error. Since the voltage vector has a

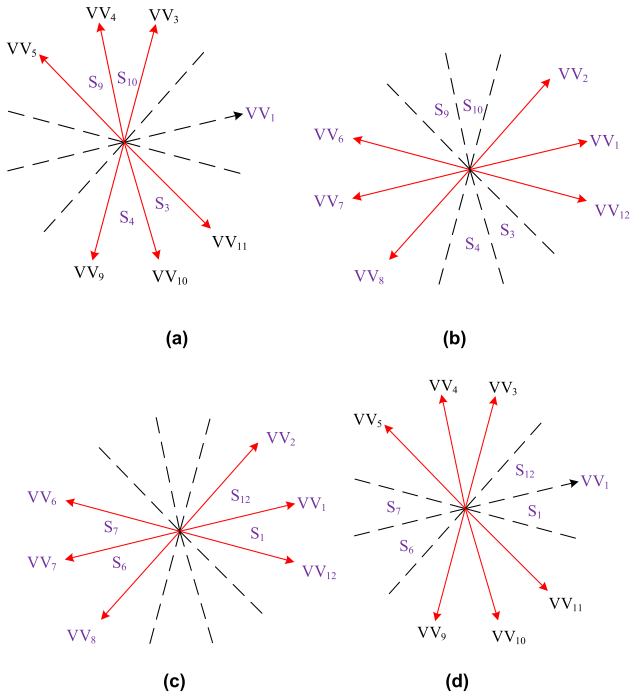

FIGURE 5. The method of selecting the voltage vector set. (a) the system changes from dynamic to steady state. (b) the system in dynamic state. (c) the system in steady state. (d) the system changes from steady to dynamic state.

TABLE 2. System states and cost function selection method.

System State	Cost function selection
From dynamics to steady state	J_1
Dynamic state	J_2
Steady state	J_1
From steady to dynamic state	J_2

little effect on the torque, the torque error can be omitted, and then the cost function is shown as follows:

$$J_1 = \left|\psi_s(k+1) - \psi_s^*\right| \tag{18}$$

Since (18) eliminates the torque component, which reduces the complexity of the system to a certain extent. In the same way, if the system is always dynamic, the voltage vector selected needs to make the torque change rapidly, and the cost function does not contain the component of the stator flux error. Since the selected voltage vector has little effect on the stator flux, the stator flux error can be omitted, and the cost function is as follows:

$$J_2 = \left|T_e(k+1) - T_e^*\right| \tag{19}$$

Table 2 shows the system states and the corresponding method of selecting the cost function. The corresponding cost function is different when the system is in different states. The four system states correspond to two cost functions.

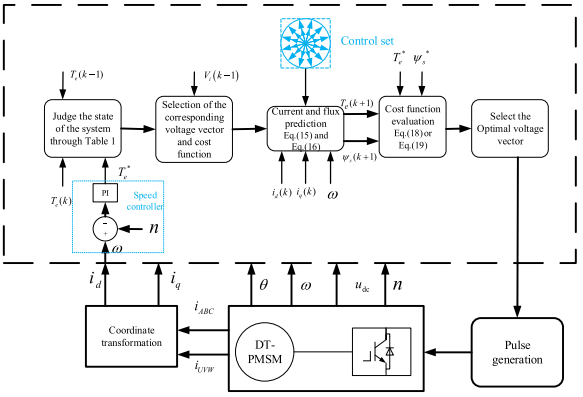

FIGURE 6. Proposed MPTC control flow.

The system flow is shown in Fig.6.

Step 1: Collect the current value, speed value, and electrical angle value through the sensor.

Step 2: Calculate the reference electromagnetic torque through the outer speed loop.

Step 3: The state of the system is obtained from Table 2. Selecting the candidate voltage vector at $(k+1)$th by describing the four principles in Fig.5, and then select (18) or (19) as the cost function.

Step 4: Bring the voltage vector, $i_d(k)$, $i_q(k)$, and ω ω into (15) and (16), which can predict the electromagnetic torque at $(k+1)$th $T_e(k+1)$ and stator flux at $(k+1)$th $\psi_s(k+1)$.

Step 5: Evaluate the candidate voltage vectors using the selected cost function.

Step 6: Select the optimal switch state through the cost function, and output a PWM signal.

D. COMPARISON BETWEEN PROPOSED METHOD AND KNOWN ONES

The comparison between the proposed method and the known method is shown in Table 3. In [31], the harmonic currents are

TABLE 3. Comparison between proposed method and known ones.

Reference	[31]	[32]	[36]	[37]	Proposed
Weighting factor	No	Yes	No	No	No
Harmonic reduction	Unified	Flux observer	V^3	V^3	V^3
Number of candidate vectors	13	6	13	3	6
Simplified prediction model	No	Yes	No	No	Yes
Computation burden	No	Reduced	No	Reduced	Significantly Reduced

not suppressed since only 12 vectors from G1 (see Fig.2), and the computational burden is almost the same as the traditional MPTC method. In [32], a flux observer method is used to suppress harmonic currents. Based on the switching table of the magnetic flux position and torque deviation, the appropriate voltage vector is preselected in the x-y and z_1-z_2 planes. The number of candidate voltage vectors is reduced to 6. However, the cost function includes a weighting factor, and there is a little reduction in the calculation burden. [36] proposes a MPTC based on the optimization of the duty period, which reduces the harmonic currents according to the V^3 method and the duty period optimization methods, and the computational burden is slightly increased compared with the traditional MPTC method. [37] greatly reduces the number of candidate vectors to 3 and cost function without weighting factor, and the calculation burden is reduced. In the method proposed in this paper, the cost function does not include weighting factor. The method also simplifies the prediction model and reduces the number of candidate voltage vectors. Compared with the above-mentioned method, the computational burden is significantly reduced.

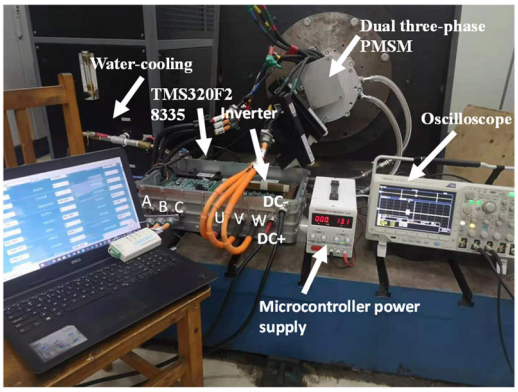

FIGURE 7. Experimental platform.

IV. EXPERIMENTAL RESULTS AND ANALYSIS

In order to verify the effectiveness of the proposed method, an experimental platform based on DSP28335 is built as shown in Fig.7. The c language code is developed in ccs6.0. In addition, the phase current is collected by a current probe (Tektronix TCO404XL), and the electromagnetic torque and speed are collected by a torque sensor (K-T40B-500Q). The waveform observation is realized by a digital storage oscilloscope (Tektronix MDO3024). The sampling frequency is set to 10 kHz. The main parameters of DT-PMSM are shown in Table 4. In this paper, the conventional MPTC method that introduces the basic voltage vector as the control set is named MPTC1. And the MPTC method that introduces the V^3 method but does not simplify the prediction model, control set, and with a weighting factor in the cost function is named MPTC2. The MPTC method proposed is named MPTC3.

TABLE 4. Parameters of DT-PMSM.

Parameter	symbol	Numerical value
Stator resistance	R_s	0.002
d-q axis inductance	L_d, L_q	0.4mH
Rated speed	n	3000 rpm
Rated torque	T_e	80 Nm
Number of pole-pairs	n_p	4

A. STEADY STATE PERFORMANCE

The steady state performance is tested under the speed of 1500 revolutions per minute (r/min) with 40N·m load. The harmonic currents of MPTC1, MPTC2, and MPTC3 are investigated. From Fig.8, it can be concluded that MPTC1 does not use the V^3 method, so the harmonic currents are relatively large. The control sets of MPTC2 and MPTC3 are the same and both use the V^3 method, the current waveform distortion is not obvious. Fig. 9 shows the fast Fourier transform analysis results of the phase currents. The phase current total harmonic distortion (THD) of the three methods is 15.44%, 6.9%, and 7.5%, respectively. The THD of phase current at the rated speed under different loads (from 0.1 to 1.0p.u of the rated load) is investigated as shown in Fig.10. The harmonic currents of MPTC1 are greater than that of MPTC2 and MPTC3 under whole load conditions.

In order to be able to analyze the torque ripple performance of the proposed method operating at different speeds, (20) shows the formula for the torque ripple in steady state.

$$T_{s\_ripple} = \sqrt{\frac{1}{n}\sum_{j=1}^{n}(T_{s\_j} - T_{s\_av})^2} \tag{20}$$

where T_{sj} is the sampled instantaneous value of torque, T_{s_av} is the sampled average value of torque, and T_{s_ripple} is the average value of torque ripple.

The generation of torque ripple is related to the control set (the more control sets, the littler the torque ripple). MPTC1 uses 12 basic voltage vectors (see G1 from Fig.2) as the control set, MPTC2 uses 12 V^3s (that is, 24 basic voltage vectors, see Fig.3) as the control set. It can be seen from Fig. 8 that compared to MPTC2, MPTC1 has a larger torque ripple. MPTC3 uses 6 V^3s (see Fig.5) as the control set. The cost function of MPTC3 does not contain the torque error component when MPTC3 is in steady state or when moving from dynamic to steady state, therefore the torque ripple is increased compared to MPTC1 and MPTC2. The torque ripple under different speeds with 98N·m load is investigated as shown in Fig.11. In the whole speed range, the torque ripple of MPTC3 is greater than MPTC1 and MPTC2.

B. DYNAMIC RESPONSES PERFORMANCE

In order to better study the control performance of the system, the dynamic response performance of the system is tested. When the motor has a load of 40N·m, the DT-PMSM speed

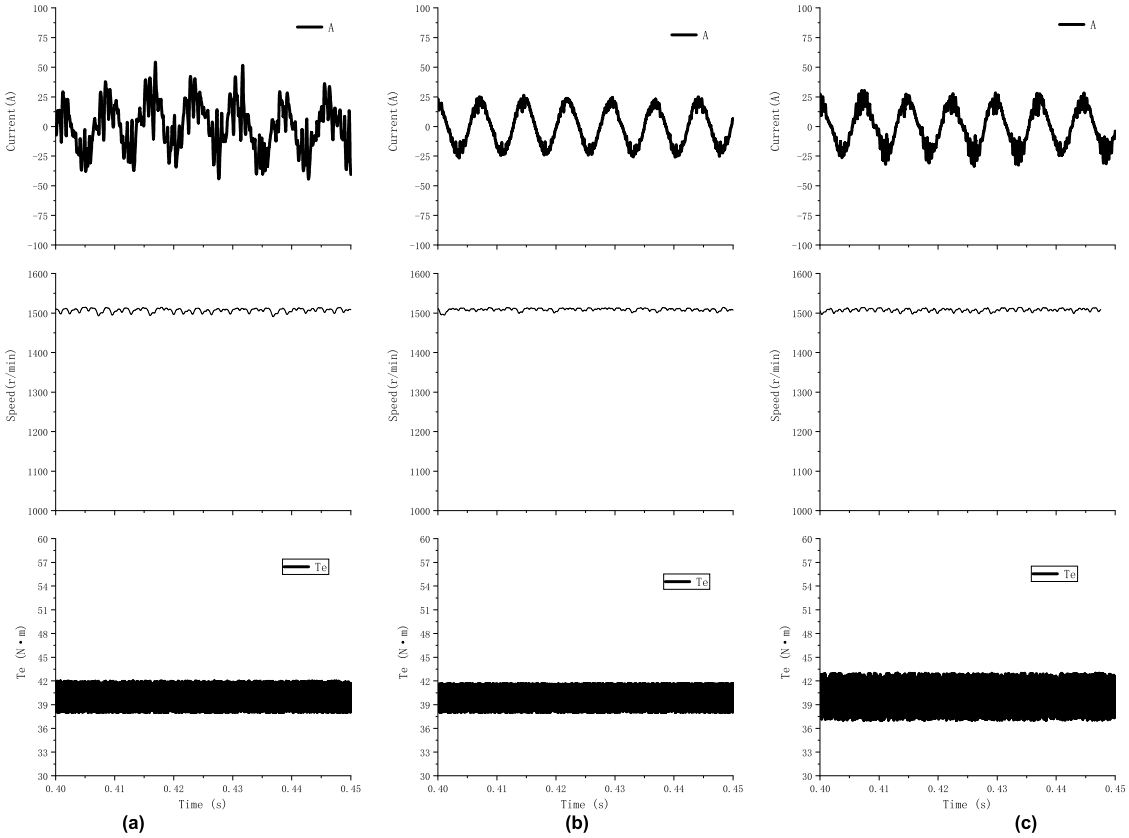

FIGURE 8. Steady state performance of the motor under 1500r/min with 40N·m load. From top to bottom: the phase current, the motor speed, and the electromagnetic torque, (a) MPTC1 (b) MPTC2 phase (c) MPTC3.

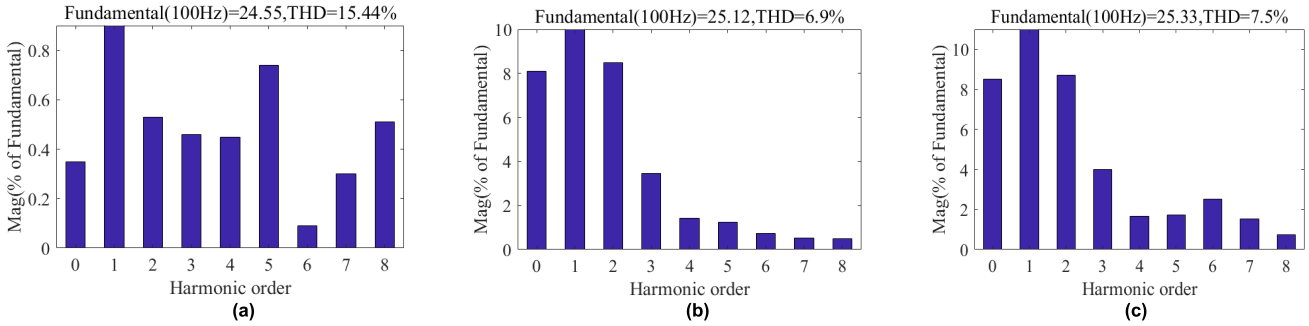

FIGURE 9. The fast Fourier transform(FFT) analysis of A-phase current. (a) MPTC1 phase current FFT analysis. (b) MPTC2 phase current FFT analysis. (c) MPTC3 phase current FFT analysis.

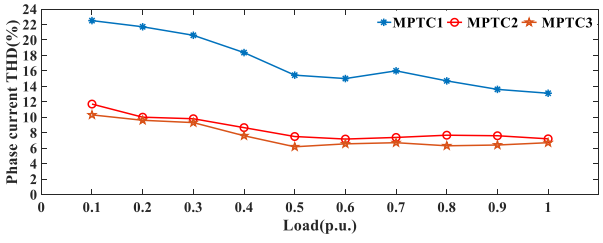

FIGURE 10. THD of A-phase current at 3000r/min under different load commands.

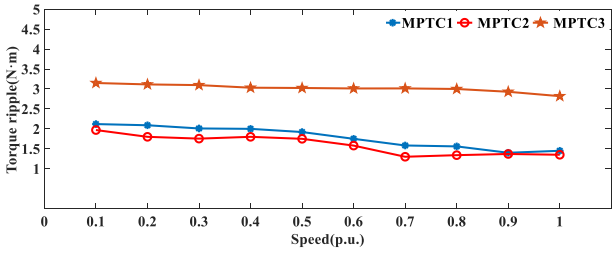

FIGURE 11. Torque performance at 98N·m under different speed commands.

is 1000r/min, and then the speed is suddenly increased to 1500r/min. Fig.12 shows the change of the phase current and the response of the speed when the DT-PMSM accelerates suddenly. For the three methods, the phase current changes smoothly, the response time is almost the same (the system

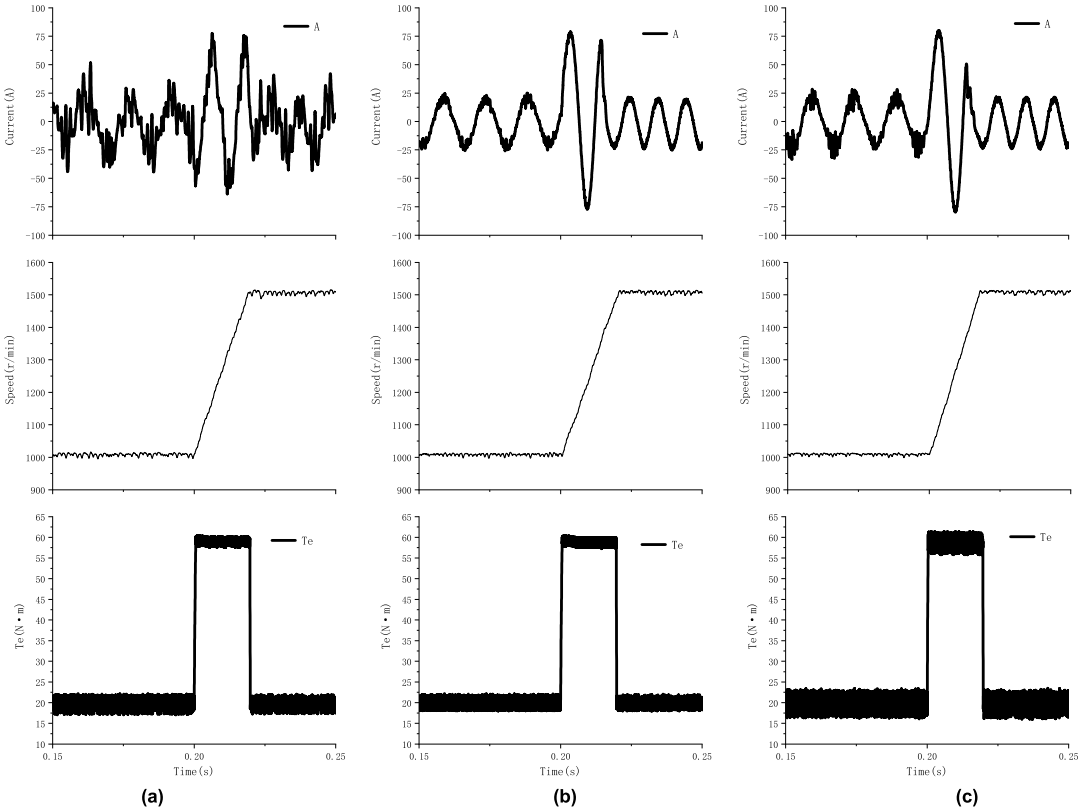

FIGURE 12. Dynamic state performance of the motor from 1000 to 1500r/min with 40N·m load. From top to bottom: the phase current, the motor speed, and the electromagnetic torque, (a) MPTC1 (b) MPTC2 (c) MPTC3.

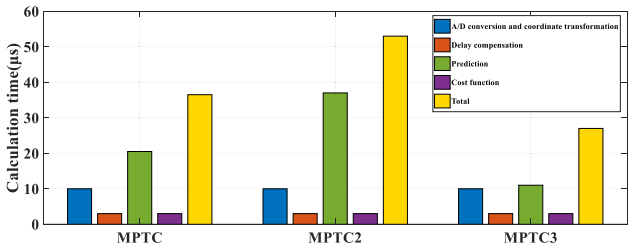

FIGURE 13. Calculation time analysis.

response time is about 220ms), and the speed curve has not an overshoot. For MPTC3, it inherits the satisfactory dynamic performance of MPTC1 and MPTC2.

C. COMPARISON OF COMPUTATIONAL BURDEN

The computational burden of the proposed method is studied. The computational burden is related to the number of candidate voltage vectors in the control set, the complexity of the prediction model. It can be seen from Fig.13 that MPTC3 takes a short time in the calculation of the prediction model. Compared with MPTC1 and MPTC2, the total calculation time of MPTC3 is greatly reduced. The total calculation time of MPTC3 is less than 30μs, which means that the switching frequency can theoretically be increased to about 33kHz. The combination of simplifying the prediction model and reducing the number of candidate voltage vectors can greatly reduce the calculation burden.

V. CONCLUSION

In this paper, a MPTC method without weighting factor is proposed and successfully applied to DT-PMSM. The contributions of this paper are as follows:

(1) The V^3 method is introduced, which can significantly reduce the harmonic currents compared with the conventional MPTC method.

(2) The cost function is selected according to the system state, eliminating the weighting factor and avoiding the problem of the difficult design of weighting factor.

(3) The methods are proposed to simplify the dual-vector prediction model and to reduce the number of candidate voltage vectors. The complexity of the prediction model is decreased and the number of candidate voltage vectors is reduced from 13 to 6, which reduces the computational burden on the CPU by combining the two methods.

The advantages of the methods proposed in this paper have all been demonstrated experimentally. At the expense of a little torque performance, the CPU is significantly less computationally burdened. The total is an execution time of about 30μs and the inverter can theoretically

operate at about 33kHz. This paper provides new ideas for dual three-phase motor applications at medium and high speeds.

REFERENCES

[1] M. Cheng, F. Yu, K. T. Chau, and W. Hua, "Dynamic performance evaluation of a nine-phase flux-switching permanent-magnet motor drive with model predictive control," *IEEE Trans. Ind. Electron.*, vol. 63, no. 7, pp. 4539–4549, Jul. 2016.

[2] F. Yu, W. Zhang, Y. Shen, and J. Mao, "A nine-phase permanent magnet electric-drive-reconstructed onboard charger for electric vehicle," *IEEE Trans. Energy Convers.*, vol. 33, no. 4, pp. 2091–2101, Dec. 2018.

[3] F. Yu, M. Cheng, and K. T. Chau, "Controllability and performance of a nine-phase FSPM motor under severe five open-phase fault conditions," *IEEE Trans. Energy Convers.*, vol. 31, no. 1, pp. 323–332, Mar. 2016.

[4] J. Fei, H. Wang, and Y. Fang, "Novel neural network fractional-order sliding-mode control with application to active power filter," *IEEE Trans. Syst., Man, Cybern. Syst.*, early access, Apr. 15, 2021, doi: 10.1109/TSMC.2021.3071360.

[5] J. Fei, Z. Wang, X. Liang, Z. Feng, and Y. Xue, "Fractional sliding mode control for micro gyroscope based on multilayer recurrent fuzzy neural network," *IEEE Trans. Fuzzy Syst.*, early access, Mar. 9, 2021, doi: 10.1109/TFUZZ.2021.3064704.

[6] J. Fei and Z. Feng, "Fractional-order finite-time super-twisting sliding mode control of micro gyroscope based on double-loop fuzzy neural network," *IEEE Trans. Syst., Man, Cybern. Syst.*, early access, Mar. 25, 2020, doi: 10.1109/TSMC.2020.2979979.

[7] J. Fei, Y. Chen, L. Liu, and Y. Fang, "Fuzzy multiple hidden layer recurrent neural control of nonlinear system using terminal sliding-mode controller," *IEEE Trans. Cybern.*, early access, Mar. 12, 2021, doi: 10.1109/TCYB.2021.3052234.

[8] F. J. Lin, K. H. Tan, and D. Y. Fang, "Squirrel-cage induction generator system using wavelet Petri fuzzy neural network control for wind power applications," *Neural Comput. Appl.*, vol. 26, no. 4, pp. 911–928, 2015.

[9] M. A. Khanesar, Y. Oniz, O. Kaynak, and H. Gao, "Direct model reference adaptive fuzzy control of networked SISO nonlinear systems," *IEEE/ASME Trans. Mechatronics*, vol. 21, no. 1, pp. 205–213, Feb. 2016.

[10] B. Yu, W. Song, Y. Guo, J. Li, and M. S. R. Saeed, "Virtual voltage vector-based model predictive current control for five-phase VSIs with common-mode voltage reduction," *IEEE Trans. Transp. Electrific.*, vol. 7, no. 2, pp. 706–717, Jun. 2021.

[11] W. Huang, W. Hua, F. Yin, F. Yu, and J. Qi, "Model predictive thrust force control of a linear flux-switching permanent magnet machine with voltage vectors selection and synthesis," *IEEE Trans. Ind. Electron.*, vol. 66, no. 6, pp. 4956–4967, Jun. 2019.

[12] X. Zhang, B. Wang, U. Manandhar, H. B. Gooi, and G. Foo, "A model predictive current controlled bidirectional three-level DC/DC converter for hybrid energy storage system in DC microgrids," *IEEE Trans. Power Electron.*, vol. 34, no. 5, pp. 4025–4030, May 2018.

[13] G. A. Papafotiou, G. D. Demetriades, and V. G. Agelidis, "Technology readiness assessment of model predictive control in medium- and high-voltage power electronics," *IEEE Trans. Ind. Electron.*, vol. 63, no. 9, pp. 5807–5815, Sep. 2016.

[14] S. Yan, J. Chen, T. Yang, and S. Y. Hui, "Improving the performance of direct power control using duty cycle optimization," *IEEE Trans. Power Electron.*, vol. 34, no. 9, pp. 9213–9223, Sep. 2019.

[15] T. Tao, W. Zhao, Y. Du, Y. Cheng, and J. Zhu, "Simplified fault-tolerant model predictive control for a five-phase permanent-magnet motor with reduced computation burden," *IEEE Trans. Power Electron.*, vol. 35, no. 4, pp. 3850–3858, Apr. 2020.

[16] P. Cortes, M. P. Kazmierkowski, R. M. Kennel, D. E. Quevedo, and J. Rodriguez, "Predictive control in power electronics and drives," *IEEE Trans. Ind. Electron.*, vol. 55, no. 12, pp. 4312–4324, Dec. 2008.

[17] C. S. Lim, E. Levi, M. Jones, N. A. Rahim, and W. P. Hew, "FCS-MPC-based current control of a five-phase induction motor and its comparison with PI-PWM control," *IEEE Trans. Ind. Electron.*, vol. 61, no. 1, pp. 149–163, Jan. 2014.

[18] P. Cortés, J. Rodríguez, D. E. Quevedo, and C. Silva, "Predictive current control strategy with imposed load current spectrum," *IEEE Trans. Power Electron.*, vol. 23, no. 2, pp. 612–618, Mar. 2008.

[19] P. Cortes, J. Rodriguez, C. Silva, and A. Flores, "Delay compensation in model predictive current control of a three-phase inverter," *IEEE Trans. Ind. Electron.*, vol. 59, no. 2, pp. 1323–1325, Feb. 2012.

[20] Q. Chen, W. Zhao, G. Liu, and Z. Lin, "Extension of virtual-signal-injection-based MTPA control for five-phase IPMSM into fault-tolerant operation," *IEEE Trans. Ind. Electron.*, vol. 66, no. 2, pp. 944–955, Feb. 2019.

[21] M. Bermudez, I. Gonzalez-Prieto, F. Barrero, H. Guzman, M. J. Duran, and X. Kestelyn, "Open-phase fault-tolerant direct torque control technique for five-phase induction motor drives," *IEEE Trans. Ind. Electron.*, vol. 64, no. 2, pp. 902–911, Feb. 2017.

[22] X. Wang, Z. Wang, and Z. Xu, "A hybrid direct torque control scheme for dual three-phase PMSM drives with improved operation performance," *IEEE Trans. Power Electron.*, vol. 34, no. 2, pp. 1622–1634, Feb. 2019.

[23] Y. Wang, X. Wang, W. Xie, F. Wang, M. Dou, R. M. Kennel, R. D. Lorenz, and D. Gerling, "Deadbeat model-predictive torque control with discrete space-vector modulation for PMSM drives," *IEEE Trans. Ind. Electron.*, vol. 64, no. 5, pp. 3537–3547, May 2017.

[24] W. Xie, X. Wang, F. Wang, W. Xu, R. M. Kennel, D. Gerling, and R. D. Lorenz, "Finite-control-set model predictive torque control with a deadbeat solution for PMSM drives," *IEEE Trans. Ind. Electron.*, vol. 62, no. 9, pp. 5402–5410, Sep. 2015.

[25] Y. Zhang and J. Zhu, "A novel duty cycle control strategy to reduce both torque and flux ripples for DTC of permanent magnet synchronous motor drives with switching frequency reduction," *IEEE Trans. Power Electron.*, vol. 26, no. 10, pp. 3055–3067, Oct. 2011.

[26] Y. Zhang and H. Yang, "Model predictive torque control of induction motor drives with optimal duty cycle control," *IEEE Trans. Power Electron.*, vol. 29, no. 12, pp. 6593–6603, Dec. 2014.

[27] C. Xue, W. Song, and X. Feng, "Finite control-set model predictive current control of five-phase permanent-magnet synchronous machine based on virtual voltage vectors," *IET Electr. Power Appl.*, vol. 11, no. 5, pp. 836–846, 2017.

[28] I. Gonzalez-Prieto, M. J. Duran, J. J. Aciego, C. Martin, and F. Barrero, "Model predictive control of six-phase induction motor drives using virtual voltage vectors," *IEEE Trans. Ind. Electron.*, vol. 65, no. 1, pp. 27–37, Jan. 2018.

[29] F. Barrero, M. R. Arahal, R. Gregor, S. Toral, and M. J. Duran, "A proof of concept study of predictive current control for VSI-driven asymmetrical dual three-phase AC machines," *IEEE Trans. Ind. Electron.*, vol. 56, no. 6, pp. 1937–1954, Jun. 2009.

[30] R. Gregor, F. Barrero, S. L. Toral, M. J. Duran, M. R. Arahal, J. Prieto, and J. L. Mora, "Predictive-space vector PWM current control method for asymmetrical dual three-phase induction motor drives," *IET Electr. Power Appl.*, vol. 4, no. 1, pp. 26–34, 2010.

[31] F. Barrero, J. Prieto, E. Levi, R. Gregor, S. Toral, M. J. Duran, and M. Jones, "An enhanced predictive current control method for asymmetrical six-phase motor drives," *IEEE Trans. Ind. Electron.*, vol. 58, no. 8, pp. 3242–3252, Aug. 2011.

[32] Y. Luo and C. Liu, "A simplified model predictive control for a dual three-phase PMSM with reduced harmonic currents," *IEEE Trans. Ind. Electron.*, vol. 65, no. 11, pp. 9079–9089, Nov. 2018.

[33] Y. Luo and C. Liu, "Elimination of harmonic currents using a reference voltage vector based-model predictive control for a six-phase PMSM motor," *IEEE Trans. Power Electron.*, vol. 34, no. 7, pp. 6960–6972, Jul. 2019.

[34] X. Wu, W. Song, and C. Xue, "Low-complexity model predictive torque control method without weighting factor for five-phase PMSM based on hysteresis comparators," *IEEE J. Emerg. Sel. Topics Power Electron.*, vol. 6, no. 4, pp. 1650–1661, Dec. 2018.

[35] W. Zhao, H. Wang, T. Tao, and D. Xu, "Model predictive torque control of five-phase PMSM by using double virtual voltage vectors based on geometric principle," *IEEE Trans. Transp. Electrific.*, early access, Mar. 2, 2021, doi: 10.1109/TTE.2021.3063193.

[36] F. Yu, X. Liu, Z. Zhu, and J. Mao, "An improved finite-control-set model predictive flux control for asymmetrical six-phase PMSMs with a novel duty-cycle regulation strategy," *IEEE Trans. Energy Convers.*, vol. 36, no. 2, pp. 1289–1299, Jun. 2021.
[37] Y. Luo and C. Liu, "Model predictive control for a six-phase PMSM motor with a reduced-dimension cost function," *IEEE Trans. Ind. Electron.*, vol. 67, no. 2, pp. 969–979, Feb. 2020.

ZHIFENG ZHANG (Member, IEEE) was born in Huludao, Liaoning, China. He received the B.Eng. degree in automation, the M.S. degree in power electronics and power drives, and the Ph.D. degree in electrical machines and apparatus from Shenyang University of Technology, Shenyang, China, in 2004, 2007, and 2011, respectively.

He is currently an Associate Professor with the School of Electrical Engineering, Shenyang University of Technology. His research interests include multi-phase permanent-magnet motor and drives.

QUANZENG SUN is currently pursuing the Ph.D. degree in electrical engineering with Shenyang University of Technology, Shenyang. His research interest includes multi-phase permanent-magnet synchronous motor control.

QISHEN DI is currently pursuing the M.Sc. degree in electrical engineering with Shenyang University of Technology. His research interests include multi-phase permanent-magnet machines and drives.

YUE WU is currently pursuing the Ph.D. degree in electrical engineering with Shenyang University of Technology. His research interests include multi-phase permanent-magnet machines and drives.